Bioorganic & Medicinal Chemistry 17 (2009) 3369–3378

Contents lists available at ScienceDirect

Bioorganic & Medicinal Chemistry

journal homepage: www.elsevier.com/locate/bmc

Molecular dynamics simulations on the critical states of the farnesyltransferase enzyme

Sérgio Filipe Sousa, Pedro Alexandrino Fernandes, Maria João Ramos *

REQUIMTE, Departamento de Química, Faculdade de Ciências, Universidade do Porto, Rua do Campo Alegre, 687, 4169-007 Porto, Portugal

ARTICLE INFO

Article history:
Received 26 November 2008
Revised 16 March 2009
Accepted 20 March 2009
Available online 2 April 2009

Keywords:
FTase
Prenyl transferases
Molecular dynamics
Amber
FTIs

ABSTRACT

Protein farnesyltransferase (FTase) is a particularly interesting zinc enzyme that promotes the transfer of a 15-carbons isoprenoid farnesyl group from farnesyl diphosphate (FPP) to a number of peptide substrates with a typical-CAAX motif at the carboxyl-terminus, where C represents the cysteine residue that is farnesylated. This enzyme has been the subject of great attention in anticancer research, as several proteins known to be involved in human cancer development are thought to serve as substrates for FTase and to require farnesylation for proper biological activity. Several FTase inhibitors have advanced into clinical testing. However, despite the progress in the field several functional and mechanistic doubts on the FTase catalytic activity have persisted. This work describes the application of molecular dynamics simulations using specifically designed molecular mechanical parameters to the four key-intermediate states formed during the FTase catalytic mechanism–FTase resting state, binary complex (FTase-FPP), ternary complex (FTase-FPP-Peptide), and product complex (FTase-Product). The study involves a comparative analysis of several important molecular aspects for which are vital not only motion but also the conformational sampling of both enzyme and substrate as well as their interaction, and especially the effect of the solvent. These include the radial distribution function of the water molecules around the catalytically important zinc metal atom, the conformations of the substrate and product molecules and the corresponding RMSF values, critical hydrogen bonds and several catalytically relevant distances. These results are discussed in light of recent experimental and computational evidence, yielding new insights into the elusive catalytic mechanism of this enzyme.

1. Introduction

Protein farnesyltransferase (FTase) is a heterodimeric Zn enzyme that catalyzes the addition of a farnesyl group from the isoprenoid donor farnesyl diphosphate (FPP), to a cysteine residue of a protein substrate containing a typical-CAAX motif at the carboxyl terminus, where C represents the cysteine residue that is farnesylated, A is an aliphatic amino acid, and X represents the terminal amino acid residue, typically alanine, serine, methionine, or glutamine.[1–5] Among the known FTase substrates are the H-, N-, and K-Ras proteins, the γ subunit of heterotrimeric G-proteins, nuclear lamins A and B, and several proteins involved in visual signal transduction.[6–8]

The discovery that farnesylation was absolutely necessary for the oncogenic forms of Ras proteins to transform cells[9–11] quickly gave rise to an escalating number of studies focusing on FTase, as the Ras family of proteins is known to be involved in something like 30% of all human cancers,[12,13] with particular high relevance in pancreatic adenocarcinomas (90%), colon adenocarcinomas and adenomas (50%), lung adenocarcinomas (30%), myeloid leukemias (30%), and melanomas (20%).[14–19]

Research in the field rapidly yielded extremely promising results, leading to a large number of patents describing FTase inhibitors (FTIs).[20] Several drugs moved into clinical testing.[21–29] However, the outcome of Phase II and Phase III clinical trials was rather disappointing, with the most advanced FTIs failing to demonstrate anti-tumour activity in Ras dependent cancers.[30,31] Interestingly, however, good results in several non-ras dependent cancers were obtained through the application of FTIs.[32–34] These finding suggests that some farnesylated proteins other than Ras must also play a role in the biological consequences of FTI treatment. However, the precise target for FTase action that is responsible for the observed anti-tumour activity is still unknown.[35] The application of FTIs in several other non-cancer related illnesses is also currently underway. Examples include malaria,[36–41] the African sleeping sickness,[42–44] Chagas disease,[45–47] Leishmaniasis,[45] and Toxoplasmosis.[48] Other emerging applications of FTase also include its use as a protein modification tool for biochemical and biotechnological purposes.[49]

In spite of the immense interest aroused by FTase, several important aspects of its catalytic mechanism have remained unex-

* Corresponding author.
E-mail address: mjramos@fc.up.pt (M.J. Ramos).

0968-0896/$ - see front matter © 2009 Published by Elsevier Ltd.
doi:10.1016/j.bmc.2009.03.055

plained or are still a matter of dispute.[50–52] An atomic-level understanding of the catalytic and inhibition mechanisms of this enzyme could help to guide the search for rationally-designed inhibitors of FTase, and would be of paramount importance in the path towards mastering FTase activity.

This study portrays an integrated molecular dynamics (MD) analysis of the four main intermediate states formed during the catalytic mechanism of FTase, in an attempt to rationalize the several events taking place at the active-site of the enzyme, including substrate binding (both FPP and the CAAX peptide) and product formation. These four key intermediates are the FTase resting state, the binary complex (FTase-FPP), the ternary complex (FTase-FPP-Peptide), and the product complex (FTase-Product) (see Fig. 1). The study uses three recent sets of parameters committed to the AMBER force field,[53,54] specifically designed to allow a reliable treatment of three different Zn coordination spheres formed during catalysis, and previously validated against 14 FTase crystallographic structures, EXAFS data, DFT, and QM/MM theoretical calculations.[55] The insights given from the set of four MD simulations performed on these key states, are analyzed in light of recent interpretations of old mechanistic dilemmas and currently existing doubts on the FTase mechanism, yielding important indications for future mechanistic studies, and contributing positively to a better understanding of the farnesylation process.

2. Results and discussion

2.1. Radial distribution function of water around zinc

The exact nature of the Zn coordination sphere in FTase has remained for years the subject of several pungent questions.[50] The existing doubts involved both the number and the identity of the ligands at the first coordination sphere and were in fact at the very heart of the atomic-level search for the FTase catalytic mechanism, as Zn plays a critical role in the whole farnesylation process.

In the first X-ray crystallographic structure of a farnesyltransferase enzyme, obtained for the resting state of FTase in 1997 (structure 1FT1),[56] the zinc coordination sphere was interpreted as being distorted pentacoordinated, with three residues from the β-subunit (Asp297β bidentate, Cys299β, and His362β), plus a

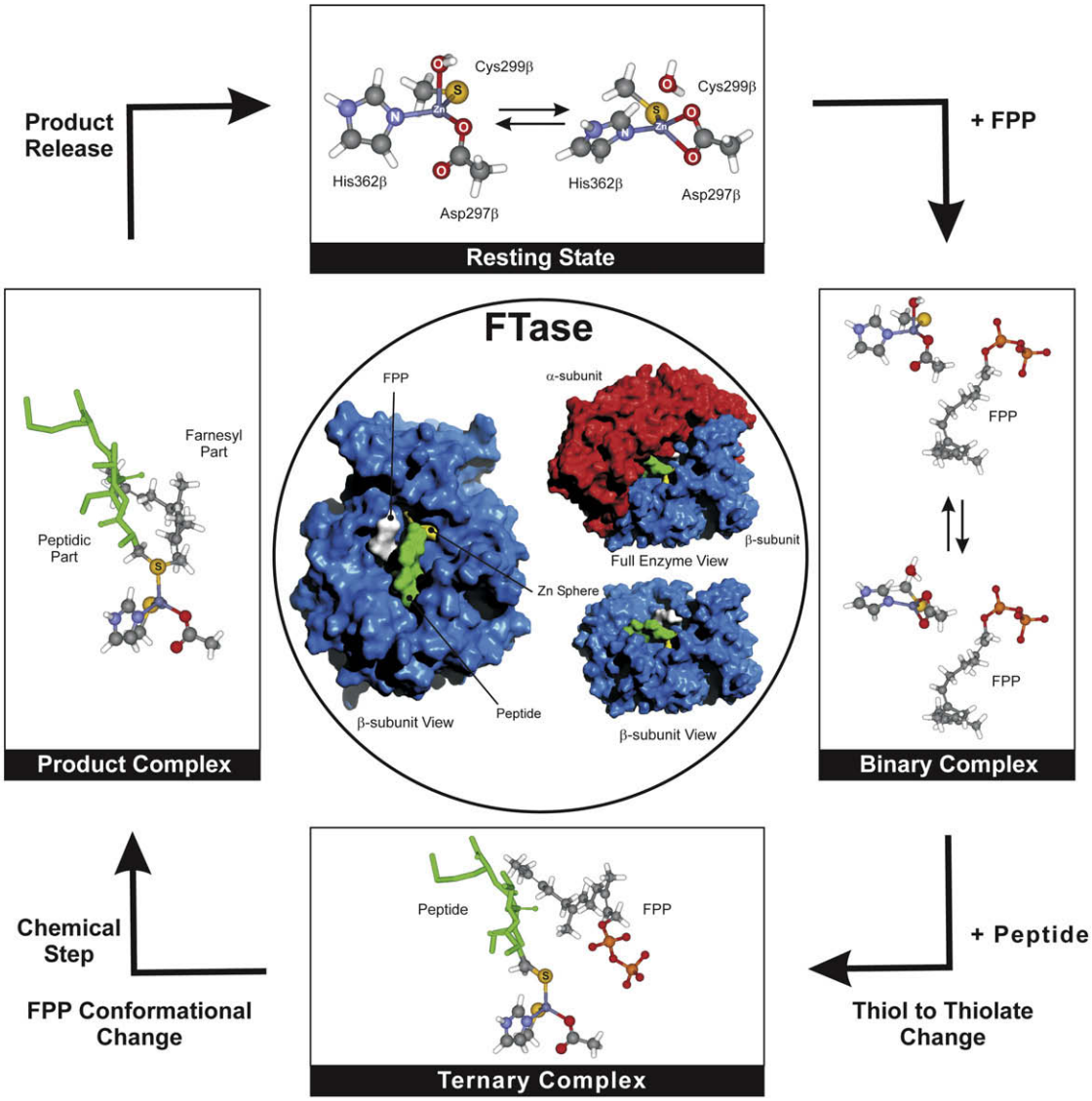

Figure 1. Schematic representation of the Zn coordination sphere in the four main intermediate states of the catalytic mechanism of FTase, illustrating the current standing of the field. The center picture illustrates the position of the metal coordination sphere, FPP molecule and peptide substrate within the context of the full enzyme at the ternary complex.

water molecule, as ligands. However, the 2.74-Å distance observed between the zinc ion and the water molecule failed to allow an unequivocal assignment of this molecule to the first coordination sphere of the metal atom, as the average bond-length for a Zn–OH_2 interaction is 2.22 Å, as recently shown in a recent analysis of Zn proteins in the PDB.[57] Furthermore, the bidentate character of the aspartate ligand in this structure (Zn–O distances of 2.00 and 2.56 Å) was also doubtful.[57] In most of the structures subsequently determined, the difference between the distances to the two carboxylate oxygens was even higher, and so was the distance between Zn and water. Therefore, considering Asp297β a bidentate ligand, assigning the water molecule to the first coordination sphere of Zn, and regarding the metal coordination sphere as pentacoordinated were three highly questionable conclusions, all of them open to debate.

Additional doubts arose from the first X-ray absorption fine structure studies (EXAFS),[58] which demonstrated that the Zn coordination sphere was in fact tetracoordinated, with three low-Z ligands (oxygen or nitrogen, in a 2.0–2.2 Å interval), plus a cysteine sulfur (Cys299β) at the resting state. Two of these three bonds with low-Z ligands were known to be formed with a His362β nitrogen atom and with an Asp297β oxygen atom. However, two candidates existed for the third Zn–(O/N) bond: the second carboxylate oxygen from Asp297β (defining an almost symmetrical bidentate ligand) or a tightly bound water molecule. To each one of these two alternatives corresponded two very different farnesylation mechanisms, since the EXAFS studies have also showed that it was this ligand that was displaced with peptide coordination to the metal coordination sphere.

The presence of a water molecule at the metal coordination sphere is an extremely common motif in Zn enzymes,[57,59,60] and in the case of FTase would implicate a mechanism where the water molecule would be replaced by the sulfur atom from the peptide substrate, eventually recovering its position at the metal sphere after the chemical step has taken place. The bidentate Asp297β hypothesis would implicate a change in the coordination form of Asp297β to monodentate with peptide coordination, with a later return to the bidentate form with product (or intermediate) release.[58]

We have previously analysed this dilemma by evaluating the two possibilities using B3LYP and B3LYP/PM3 approaches.[61] To our surprise we have found that not only the two coordination alternatives were possible and were located at a remarkably close energetic proximity, but also that the conversion between the two was reversible and extremely fast, suggesting the existence of an equilibrium at room temperature between the water-bound minimum and the bidentate minimum at the resting of the enzyme (see Fig. 1).

Following this conclusion, we have analyzed some of the mechanistic paradoxes of FTase within a carboxylate-shift paradigm.[62–65] We have also explored this type of monodentate to bidentate changes with concomitant exit of a small ligand for a variety of different molecules and for several different Zn coordination spheres, representing different Zn biological systems.[66]

Taking into consideration our previous computational work and the massive set of experimental results, we can rationalize the available data on a mechanistic proposal for the FTase catalytic mechanism where the enzyme exists at the resting state as an equilibrium between a water-bound monodentate form and a bidentate form with the water molecule free[61] (see Fig. 1); FPP then binds to a hydrophobic cavity of the enzyme near the catalytic Zn ion, but without altering the metal coordination sphere, which remains an equilibrium of two conformations; Peptide binding then proceeds, with the cysteine sulfur atom coordinating the metal coordination sphere in the thiol form, and substituting the water molecule in a process where the bidentate form acts as an intermediate;[63] the Zn-bound peptide thiol substrate then loses a proton to an active-site base or to the solvent, yielding a tightly-bound Zn thiolate;[58,63] the transfer of the farnesyl moiety from FPP towards the peptide substrate involves a rotation of the first isoprenoid subunit, which positions the FPP carbon 1 at a distance of around 5–5.5 Å away from the Zn-bound sulfur atom of the peptide substrate;[65,67,68] from this position onwards the reaction takes place with more or less simultaneous formation of the Farnesyl(C1)–S bond and breaking of the Farnesyl(C1)–PPi bond (where PPi is the pyrophosphate moiety), but without rupture of the Zn–S bond, leading to the formation of a Zn-bound farnesylated peptide (the product), in a step where a Mg^{2+} ion is thought to play an important role by stabilizing the formation of the PPi molecule; product displacement from the Zn coordination sphere takes place through a carboxylate-shift mechanism, in a low-barrier step where Asp297β changes from the monodentate to the bidentate coordination form;[64] the farnesylated peptide product is then displaced to an hydrophobic pocket outside the active site, which corresponds to a 8–9 Å distance between zinc and the thioether sulfur atom; finally product release is the rate-limiting step and is promoted by the entrance of an additional substrate molecule.

Our MD parameters consider the Zn coordination sphere in the FTase resting state and binary complex as a tetracoordinated complex with a bidentate aspartate ligand, without a Zn-bound water molecule. Obviously, the specific nature of MD methods in general, and particularly the use of a bonded potential in the parameterization of the metal sphere,[55] forecloses a direct analysis of an equilibrium between the bidentate aspartate ligand and the Zn-water-bound form, as bond forming and bond breaking events are not accounted for. However, the mechanistic proposal outlined above admits the existence of a water molecule in the FTase resting state and binary complex (FTase-FPP) at an appropriate distance from the Zn coordination sphere for that an equilibrium between a water-unbound bidentate form and a water-bound monodentate

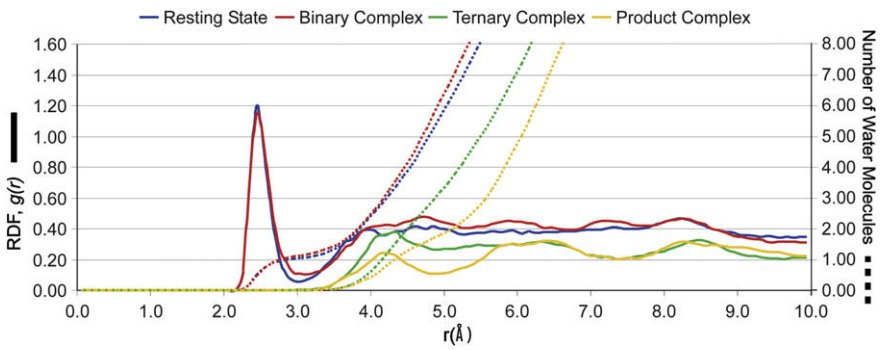

Figure 2. Radial distribution functions (RDFs,) and number of water molecules as a function of the distance to Zn, calculated from the MD simulations for the four-key states of the FTase catalytic mechanism: FTase resting state, binary complex (FTase-FPP), ternary complex (FTase-FPP-CVIM), and product complex (FTase-Product).

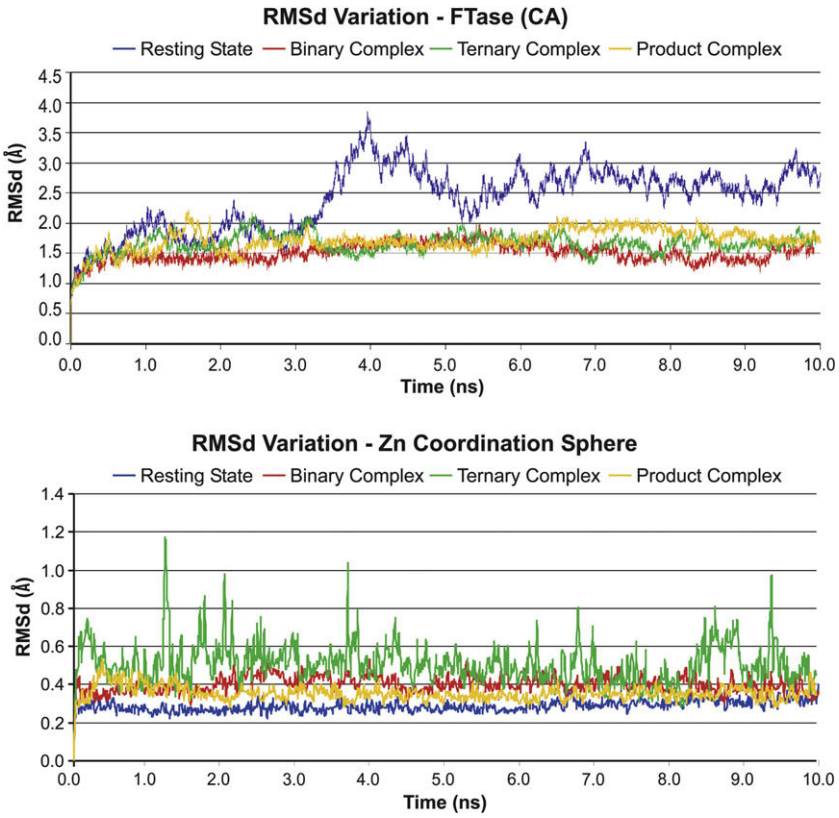

Figure 3. Graphical representations of the root mean square deviation (RMSd) variation in the MD simulations performed for the four systems considered: FTase resting state, binary complex, ternary complex, and product complex.

form may be established, and this feature can be accurately evaluated from the full MD simulations performed.

To achieve this, we have analyzed the radial distribution function (RDF) of water (from the water oxygen atom) around Zn in the four catalytic states of the enzyme considered in this study: resting state, binary complex, ternary complex, and product complex (Fig. 1). Results are presented in Figure 2. The results confirm the existence of an RDF maximum at an appropriate distance from the metal atom in order that such equilibrium can take place, both in the case of the resting state of FTase and of the binary complex. The same was, however, not observed for the ternary and product complexes, as expected. Additionally, the Zn–OH_2 radius within which a water molecule can be found on average is of 2.8 Å for the resting state and binary complex, whereas for the other two states of the enzyme is of 4.2 and 4.3 Å, respectively for the ternary and product complexes.

These results illustrate the existence of intrinsic differences in the solvation shells of Zn in the four catalytic states of FTase that partially determine the metal coordination spheres that are able to exist as an equilibrium between a water-bound monodentate form and a water-unbound bidentate form (via Carboxylate-shift). There is still another important difference that is evident from the RDF analysis performed on these four intermediate states: in the resting state and binary complex, the RDF analysis yield a sharp peak around 2.5 Å (Fig. 3). This sharp peak indicates the existence of a specific interaction between the Zn cation and the water–oxygen atom. In the ternary and product complex, however, the existing peaks are much less pronounced (Fig. 3), suggesting that the water molecules occupy almost all the free-surrounding volume, without being structurally oriented by the Zn metal atom. No significant interaction between Zn and the water molecules exists in these two states. The conclusions drawn a this level, are also in agreement with previous computational work, done at the quantum mechanical level on the energetics of the metal coordination sphere[61,63,64] and with available EXAFS results.[58]

2.2. MD overall results

Table 1 lists the average root mean square deviation (RMSd) for the backbone C_α atoms (CA) and for the Zn coordination sphere determined from the instantaneous values collected at every 0.2 ps during the 10 ns of simulation time for each of the four FTase states considered: FTase resting state, binary complex (FTase-FPP), ternary complex (FTase-FPP-CVIM), and product complex (FTase-Product) (Fig. 1). Only the values obtained after the initial 500 ps of simulation were considered in this averaging.

Figure 3 illustrates the CA and Zn coordination sphere RMSd variation with time in all the MD simulations performed. The results show that the four systems are well equilibrated and that the CA atoms are maintained within a RMSd of 2.5 Å practically throughout the entire simulation. From Table 1 and Figure 3 it is also evident that the geometries of the Zn coordination spheres were maintained very well during the entire simulation time.

Table 1
Root mean square deviation (RMSd) summary of the simulations performed (after the initial 500 ps) in relation to the corresponding crystallographic structures

RMSd (Å)	Resting state	Binary complex	Ternary complex	Product complex
CA	2.4 ± 0.5	1.5 ± 0.2	1.7 ± 0.2	1.7 ± 0.3
Zn Sphere	0.33 ± 0.06	0.38 ± 0.07	0.56 ± 0.13	0.36 ± 0.06

Table 2
Summary of the root mean square deviation (RMSd) values of the simulations performed (after the initial 500 ps) calculated for FPP, the farnesyl group, the pyrophosphate group and the CVIM peptide in relation to the corresponding crystallographic structures

RMSd (Å)	Resting state	Binary complex	Ternary complex	Product complex
FPP	—	2.4 + 0.2	1.2 + 0.2	—
Farnesyl	—	2.3 + 0.3	1.2 + 0.2	1.1 + 0.3
Pyrosphosphate	—	1.1 + 0.2	0.3 + 0.3	—
CVIM	—	—	1.3 + 0.2	1.8 + 0.3

2.3. Substrate conformations

Following the analysis of the radial distribution functions of the water molecules around Zn in the four FTase intermediate states, we have dedicated our attention to a comparative analysis of the behaviour of the several individual substrate/product components in the FTase resting state, binary complex, ternary complex, and product complex. In particular, we have focused this analysis on Zn, the full FPP substrate molecule, the farnesyl portion of FPP and of the farnesylated product, the pyrophosphate moiety of FPP, and the CVIM motif at both the peptide substrate and farnesylated product.

Table 2 lists the average root mean square deviation (RMSd) values for all the atoms in each of these molecular elements determined from the instantaneous values collected at every 0.2 ps during the 10 ns of simulation time for each of the four FTase states considered. Table 3 presents the corresponding root mean square fluctuation (RMSF) values, which illustrate the average displacement (i.e., the positional variation) of each one of these elements in relation to their average structure over the whole simulation (after the initial 500 ps), thereby giving an indication of the relative flexibility that characterizes each of these components.

Table 2 shows that the structural elements considered in this analysis all maintain their positions in relation to the corresponding crystallographic structures. Table 3 further shows that the positional variation (RMSF) of Zn is greatly decreased from the resting state and binary complex to the ternary complex (ca. 30%), and remains low at the product complex.

Figure 4 shows the average conformation of the FPP molecule in the binary complex (FTase-FPP) and ternary complex (FTase-FPP-Peptide) with the indication of the most relevant hydrogen bonds formed between the pyrophosphate moiety of FPP and the enzyme. The figure highlights the difference in the coordination mode of FPP in the two states as observed in the corresponding MD simulations. The differences observed are in agreement with the substrate coordination modes reported in the PDB structures used in the preparation of the models for the two simulations, that is, the X-ray crystallographic structures with the best resolution available for the binary and ternary complexes of FTase (1FPP[69] and 1JCR[70]).

Table 3
Summary of the root mean square fluctuation (RMSF) values of the simulations performed (after the initial 500 ps) calculated for Zn, FPP, the farnesyl group, the pyrophosphate group and the CVIM peptide

RMSF (Å)	Resting state	Binary complex	Ternary complex	Product complex
Zn	0.54	0.57	0.41	0.39
FPP	—	0.99	0.98	—
Farnesyl	—	1.05	0.97	0.98
Pyrosphosphate	—	0.72	1.04	—
CVIM	—	—	1.08	0.75

Table 3 shows that the flexibility of the full FPP molecule at the binary and ternary complexes, given by the RMSF, is roughly the same. Hence, the different conformation of the FPP molecule in these two states (Fig. 4) and the presence or absence of the peptide substrate does not alter the global flexibility of the FPP molecule. The flexibility of the farnesyl portion of FPP, however, decreases from 1.05 Å to 0.97 Å between these two states, but is not further altered with the formation of the farnesylated peptide product at the product complex. The pyrophosphate moiety, experiences a major increase in the RMSF value from the binary complex to the ternary complex (>40%). Hence, peptide coordination induces an increase in the flexibility of the pyrophosphate moiety, although decreasing the flexibility of the farnesyl portion of FPP. This higher positional variation could be important for the chemical step that is catalyzed by the enzyme, which involves pyrophosphate exit, and a conformational rearrangement of the first two isoprenoid subunits of FPP, a change that is maximal for the pyrophosphate bound carbon 1 of the farnesyl portion of FPP, which is ultimately connected to the Zn-bound sulfur atom of the peptide's cysteine to yield the farnesylated peptide product.[65] FPP binding to FTase has also been anticipated to be important for the binding of several promising FTIs, as recently demonstrated in solution for Lonafarnib.[71]

Tables 4 and 5 describe the most relevant hydrogen bonds formed between the pyrophosphate moiety of FPP and the active-site amino acid residues at the FTase binary and ternary complexes, respectively. Only the hydrogen bonds that were present during more than 5% of the total simulation time are included. From the analysis of these two tables an immediate difference arises—it concerns the total number of hydrogen bonds between the pyrophosphate moiety and the enzyme in the two states. In the binary complex most of the hydrogen bonds of the pyrophosphate moiety are established with rapidly exchanging water molecules. The number of hydrogen bonds present during more than 5% of the simulation is therefore very small. The most important of these interactions, present during 40.7% of the simulation, is established between the O1A oxygen atom of the pyrophosphate and the highly-conserved amino acid residue His149β.

In the ternary complex on the other hand, the pyrophosphate moiety is more closely packed in a positively charged pocket located at the active-site, defined by residues Lys164α, His248β, Arg291β, Lys294β and Tyr300 β, and significantly less exposed to the solvent. The hydrogen bonds formed are thus less transient than in the case of the binary complex. Accordingly, instead of only two hydrogen bonds present during more than 5% of the simulations, a total of 19 hydrogen bonds can be identified. The active-site amino acid residues responsible for these interactions are, in order of the corresponding percentages of occupancy, Arg291β (66.7%), Lys164α (37.7%), Lys294β (31.9%), Tyr300β (13.7%), and His248β (6.2%). Some of these residues establish more than one important hydrogen bond. In particular Arg291β has three hydrogen bonds with a percentage of occupancy above 30%, whereas Lys164α and Lys294β have also three hydrogen bonds each with a percentage of occupancy above 15%. These three amino acid residues are responsible for most of the hydrogen bonds that stabilize the pyrophosphate moiety at the ternary complex. In addition to these active-site amino acid residues, there is also an important water molecule that establishes a strong hydrogen bond with the O3B pyrophosphate oxygen. This hydrogen bond is present during 67.7% of the simulation and is the most prevalent of these interactions with the pyrophosphate moiety. It is also the hydrogen bond with the shortest average distance (2.73 ± 0.12 Å) and with the longest average lifetime (14 ps). The inclusion of this conserved water molecule seems therefore paramount for a correct description of pyrophosphate binding in the FTase active-site and for the modelling of the chemical step in the reaction catalyzed by this enzyme,

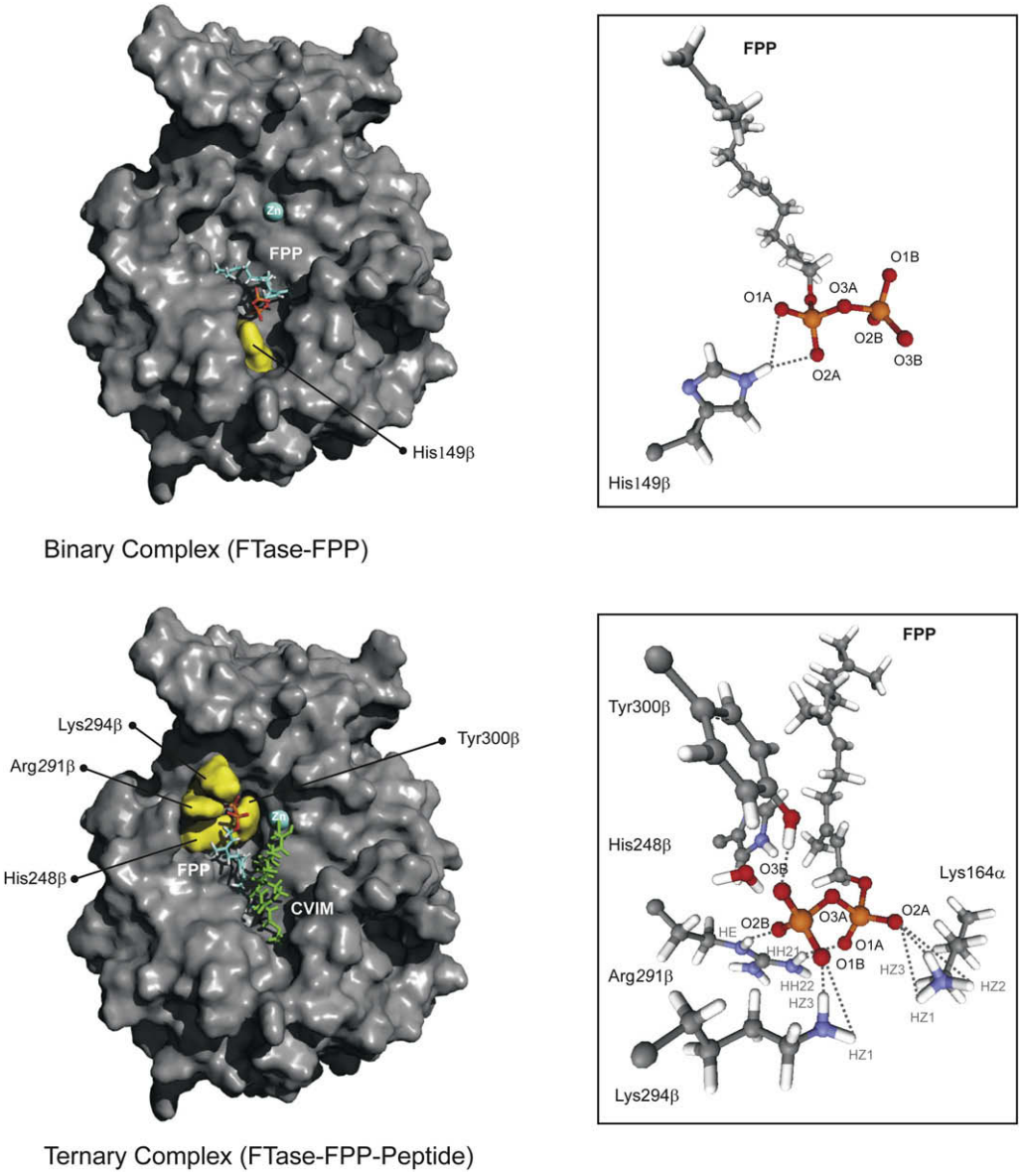

Figure 4. Schematic representation of the FPP conformation in the binary complex (FTase-FPP) and ternary complex (FTase-FPP-Peptide) with the indication of the most relevant hydrogen bonds formed between the pyrophosphate moiety of FPP and the enzyme. For clarity purposes only the molecular surface of the β-subunit is shown.

Table 4
Summary of the most relevant hydrogen bonds (i.e., those present during more than 5% of the simulation) formed between the pyrophosphate moiety of FPP and the active-site amino acid residues at the FTase binary complex (only the hydrogen bonds that were present during more than 5% of the total simulation time are included)

Donor atom	Acceptor			Distance (Å)	Angle (°)	Average lifetime (ps)	% Ocuppied
	Residue	Atom 1	Atom 2				
O1A	His149β	HE2	NE2	2.86 ± 0.09	148 ± 12	2.6	40.7
O2A	His149β	HE2	NE2	2.90 ± 0.07	159 ± 10	1.6	6.32

which involves the transfer of the farnesyl group to the Zn-bound sulfur atom of the cysteine residue in the peptide substrate, with concomitant pyrophosphate exit.

Figure 5 shows the conformation of the CVIM peptide at the FTase ternary complex and at the FTase product complex (i.e., in the farnesylated peptide). The average position occupied by this molecule in the MD simulations is not significantly altered with product formation, as reported in the initial X-ray structures.[70,72,73] From the analysis of Table 3 it is however evident that the flexibility of the CVIM peptide is significantly decreased with the formation of the farnesylated product (by 30%), an observation that contrasts with the invariability observed for the farnesyl moiety, which comprises the remainder of the farnesylated product molecule.

Table 5
Summary of the most relevant hydrogen bonds (i.e., those present during more than 5% of the simulation) formed between the pyrophosphate moiety of FPP and the active-site amino acid residues at the FTase ternary complex

Donor atom	Acceptor			Distance (Å)	Angle (°)	Average Lifetime (ps)	% Ocuppied
	Residue	Atom 1	Atom 2				
O2A	Lys164α	HZ3	NZ	2.80 ± 0.09	153 ± 14	5.4	37.7
O2A	Lys164α	HZ2	NZ	2.79 ± 0.09	152 ± 14	4.2	16.7
O2A	Lys164α	HZ1	NZ	2.80 ± 0.10	152 ± 14	4.4	15.9
O1A	Lys164α	HZ3	NZ	2.88 ± 0.09	152 ± 14	1.5	5.4
O2B	His248β	HE2	NE2	2.90 ± 0.08	160 ± 11	1.2	6.2
O2B	Arg291β	HE	NE	2.81 ± 0.09	156 ± 10	11.9	66.7
O1A	Arg291β	HH21	NH2	2.84 ± 0.10	142 ± 12	2.9	53.0
O2B	Arg291β	HH21	NH2	2.86 ± 0.09	141 ± 8	2.4	31.3
O1A	Arg291β	HE	NE	2.85 ± 0.09	154 ± 9	4.6	12.5
O2A	Arg291β	HH21	NH2	2.87 ± 0.09	152 ± 11	2.2	8.4
O1B	Arg291β	HE	NE	2.82 ± 0.09	156 ± 11	8.6	7.3
O1B	Lys294β	HZ3	NZ	2.77 ± 0.10	145 ± 14	4.0	31.9
O1B	Lys294β	HZ2	NZ	2.77 ± 0.10	145 ± 14	3.6	19.8
O1B	Lys294β	HZ1	NZ	2.76 ± 0.09	144 ± 14	3.8	17.1
O2B	Lys294β	HZ3	NZ	2.86 ± 0.09	151 ± 13	1.7	9.9
O2B	Lys294β	HZ2	NZ	2.84 ± 0.09	150 ± 13	1.7	6.8
O2B	Tyr300β	HH	OH	2.78 ± 0.12	171 ± 10	4.0	13.7
O3A	Tyr300β	HH	OH	2.89 ± 0.08	129 ± 10	1.3	7.9
O3B	H_2O	HH	OH	2.73 ± 0.12	162 ± 10	14.0	67.7

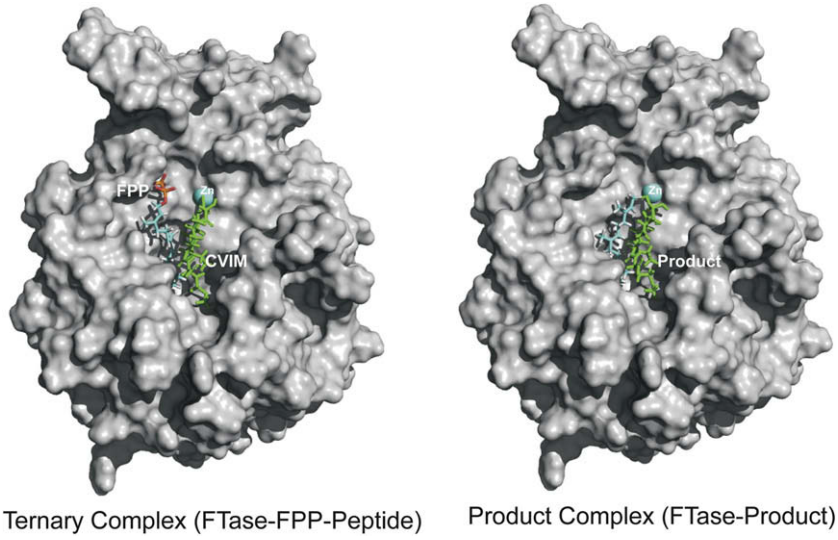

Figure 5. Schematic representation of the conformation of the FPP and CVIM substrates at the FTase ternary complex and of conformation of the farnesylated product at the FTase product complex. For clarity purposes only the molecular surface of the β-subunit is shown.

2.4. Analysis of some important distances

To complement this MD analysis on the four main intermediate states of the catalytic mechanism of FTase, the average values and the corresponding standard deviation of a series of potentially important distances, from the catalytic point of view, were calculated and compared for the ternary and product complex. These comprise the distance between the Zn-bound peptide's cysteine sulfur atom and nine possible active-site proton acceptors, namely Lys164α, Asp297β, Tyr300β, Asp352β, Lys353β, Lys356β, Asp359β, Tyr361β, and Tyr365β, which eventually could act as a base to receive the proton from the Zn-bound thiol to yield a Zn-bound thiolate.[50,63,74–77] The values determined from the MD simulations are presented in Table 6 together with the corresponding distances in the X-ray crystallographic structures that refer to each intermediate state. The values indicated in Table 6 show a good agreement between the MD simulations performed and the several X-ray crystallographic structures available for each complex.

The identity of the base that receives the thiol proton upon the change from a zinc-bound thiol to a zinc-bound thiolate remains one of the unsettled issues in the FTase catalytic mechanism.[50,63] The solvent would be the first natural option. However, as demonstrated in the radial distribution function analysis of the water molecules around Zn, FPP coordination and the subsequent entrance of the peptide substrate greatly limit direct access to solvent molecules. Two active-site residues have been discussed and dismissed in the literature as possible proton acceptors. Tyr300β was the first candidate suggested[78] (average distances of 5.30 ± 0.46 Å and 5.30 ± 0.30 Å in the MD simulations, (Table 6). Initial mutagenesis studies seemed to confirm this hypothesis by

Table 6
Comparison of the average molecular dynamics values of a series of catalytically relevant distances (calculated after the initial 500 ps of simulation) with the corresponding values in the related X-ray crystallographic structures (resolution indicated in parenthesis, in Å)

Distances evaluated	Ternary complex					Product complex		
	MD Simulation	1QBQ (2.40)	1D8D (2.00)	1JCR (2.00)	1JCS (2.20)	MD Simulation	1KZP (2.10)	1O1T (2.10)
S (Cys, Peptide)–N (Lys164α)	6.87 ± 1.71	7.13	5.71	8.26	6.65	10.55 ± 1.30	8.17	7.76
S (Cys, Peptide)–O1 (Asp297β)	3.10 ± 0.17	3.15	3.13	3.50	3.20	3.17 ± 0.17	3.29	3.29
S (Cys, Peptide)–O2 (Asp297β)	4.60 ± 0.15	4.63	4.71	4.83	4.67	4.75 ± 0.14	4.79	4.88
S (Cys, Peptide)–O (Tyr300β)	5.30 ± 0.46	5.71	5.12	5.09	5.10	5.30 ± 0.30	5.92	5.78
S (Cys, Peptide)–O1 (Asp352β)	5.21 ± 1.09	4.90	4.92	5.48	5.08	5.76 ± 0.30	4.99	5.17
S (Cys, Peptide)–O2 (Asp352β)	5.53 ± 0.76	6.36	6.04	6.61	6.12	5.87 ± 0.60	6.22	6.39
S (Cys, Peptide)–N (Lys353β)	7.35 ± 0.49	8.07	7.62	8.27	7.77	7.91 ± 0.48	7.84	7.80
S (Cys, Peptide)–N (Lys356β)	7.50 ± 1.53	7.46	6.75	8.36	7.40	10.29 ± 1.35	8.13	7.68
S (Cys, Peptide)–O1 (Asp359β)	7.23 ± 0.32	6.99	6.81	6.85	6.75	7.32 ± 0.31	6.73	7.06
S (Cys, Peptide)–O2 (Asp359β)	7.42 ± 0.45	7.14	7.28	7.15	7.34	7.52 ± 0.48	7.33	7.44
S (Cys, Peptide)–O (Tyr361β)	5.52 ± 0.41	4.76	4.92	4.22	4.83	5.23 ± 0.36	4.99	4.86
S (Cys, Peptide)–O (Tyr365β)	11.31 ± 0.59	11.07	11.32	10.38	10.93	11.20 ± 0.41	11.37	11.29

showing that upon peptide binding in Y310βF yeast mutant (Tyr310β in yeast FTase corresponds to Tyr300β in the mammalian enzyme) the acidity of what seemed a thiol in a bound peptide was enhanced 1 pK_a unit less than in the wild type FTase.[77] However, subsequent mutagenesis studies have shown that the pH dependence curves with peptide entrance were independent of the existence of a hydroxyl group at this position, therefore ruling out any eventual role of this tyrosine residue in cysteine thiol deprotonation.[76] This last study, when considering the K164Aα mutant, demonstrated the existence of an altered pH dependence of peptide binding and a decreased affinity for the protonated peptide, although exhibiting a similar affinity for the deprotonated species.[76] An analysis of the 4 crystallographic structures of the FTase ternary complex with a peptide substrate and an FPP molecule (or analogue) (PDB codes 1QBQ, 1D8D, 1JCR, and 1JCS)[70,73,79] renders an average distance of 6.94 Å between the peptide's cysteine sulfur and the nitrogen atom from Lys164α. The value calculated from the MD simulation on the ternary complex is of 6.87 ± 0.96 Å, whereas for the product complex a value of 10.55 ± 1.30 Å was found. Despite the large standard deviation obtained from the MD simulations for this distance and the large differences reported between the several X-ray structures, the range of values obtained is too large for direct interaction, suggesting that, if in fact the peptide binds zinc as a thiol, the role of Lys164α would lie probably only in stabilizing the coordination of thiol and the pyrophosphate moiety[76] and not in accepting the proton.

Residues Lys353β, Lys356β, Asp359β, and Tyr365β are at an even larger average distance from the Zn-bound sulfur atom (Table 6). A direct role by such residues in thiol deprotonation, even in a process mediated by a single water molecule is therefore unlikely. Three residues were identified at distances of less than 6 Å from the Zn-bound sulfur atom: Asp297β, Asp352β, and Tyr361β. Asp297β is a key Zn-binding residue[80–82] that assists substrate binding and product exit events through a carboxylate-shift mechanism (monodentate to bidentate change and vice-versa),[64–66] whereas Asp352β has been suggested to act as a magnesium ligand.[83] The participation of the carboxylate side chain of these residues seems therefore also very unlikely. The Tyr361β residue on the other hand seems conceptually a more likely alternative. An analysis of the 4 crystallographic structures already mentioned for the ternary complex (pdb codes 1QBQ, 1D8D, 1JCR, and 1JCS) and of the average MD simulation distances (Table 6) reveals that this residue is in general at a smaller distance from the zinc bound sulfur atom than the other two residues previously discussed in the literature as possible proton acceptors (i.e., Tyr300β and Lys164α).

We have also searched for possible intrinsic features of the enzyme that could facilitate an acid/base role by the Tyr361β residue. The 4 crystallographic structures analyzed all show the existence of a very strong hydrogen bond between Tyr361β and Trp303β. In fact, in these structures the distance between the tyrosine oxygen atom and the tryptophan nitrogen atom is very small and remarkably similar, with values ranging from 2.81 Å to 2.87 Å. The MD simulations performed are also in line with this observation, although the neutral protonation state used to model the tyrosine residue in the simulations forecloses a direct comparison. Globally, these features suggest that Tyr361β could be stabilized by Trp303β as an ionized tyrosinate, ready to receive a proton from the zinc-bound cysteine thiol. Furthermore, these structural aspects could implicate Trp303β as a crucial residue in a complex hydrogen bond network which would deprotonate the cysteine thiol to Tyr361β, and ultimately transfer the proton to a free solvent molecule or even to one of the oxygens of the pyrophosphate moiety from the FPP substrate.

A number of mutagenesis studies have analyzed the effect of Tyr361β.[78,84–86] The role of Trp303β has also been previously explored.[81] However, the results have been inconclusive for these two residues, and in some studies even contradictory. Several studies have demonstrated that Tyr361β plays an important role in peptide binding.[69,78,84,86] However, no pH dependence studies of substrate binding were performed in mutant species at this position. A possible role in product release has also been suggested.[85] Interestingly, this residue is not conserved in the related enzyme geranylgeranyltransferase I (GGTase I) where it has been replaced by a residue that also possesses a hydroxyl group—a serine.[78] GGTase I, which is thought to follow a very similar mechanism, uses geranylgeranyl diphosphate (GGPP) as the isoprenoid donor (instead of FPP) and catalyzes the prenylation of CAAX substrates where X is typically leucine.[2] Mutagenesis studies at the Trp303β position are also coherent with a possible role in peptide coordination.[81] More experimental and computational studies are necessary to confirm the identity of Tyr361β as the proton acceptor.

3. Conclusions

In this study, the application of molecular dynamics simulations with the three sets of molecular mechanical parameters specifically designed to allow a reliable treatment of the several Zn coordination spheres formed during catalysis enabled a comparative analysis of a series of catalytically relevant features for which the influence of the atomic and molecular motion is essential, or at least, of great importance.

In particular, the analysis of the radial distribution functions of the water molecules around Zn in the four key-intermediate states demonstrated the existence of intrinsic differences in the solvation shells of the metal. At the enzyme resting state and binary complex

there is typically a water molecule at an average interacting distance of 2.8 Å from the metal atom, which in practice enables the existence of an equilibrium between a water-bound monodentate (Asp297β) form and a water-unbound bidentate form, as previously suggested from computational work at the quantum level with small active-site models[61,63] and experimental EXAFS results.[58] In the ternary and product complexes, however, the average interaction distance for the first solvation shell is significantly higher (4.2–4.3 Å), foreclosing a carboxylate shift equilibrium such as the one outlined for the resting state and binary complex. These features could be of particular interest for drug development efforts, as targeting the interaction with the catalytic Zn ion to develop more potent FTase inhibitors is one of the strategies currently underway.[87]

This study has also shown that peptide coordination results in a very important increase in the flexibility of the pyrophosphate moiety of FPP, while simultaneously decreasing that of the farnesyl portion. This unusually high increase in the positional variation of the pyrophosphate moiety may be of relevance for the chemical step, a process in which the pyrophosphate bound carbon 1 experiences a major conformational change, ultimately resulting in the formation of a bond between this atom and the Zn-bound peptide sulfur atom, with simultaneous exit of the pyrophosphate moiety.

In addition, the analysis of the hydrogen bonds surrounding the pyrophosphate moiety of the FPP molecule at the FTase binary and ternary complex has shown two rather different hydrogen bonding patterns. At the binary complex most of these interactions are established with rapidly exchanging water molecules. The only exception is the highly-conserved amino acid residue His149β. At the ternary complex however the hydrogen bonds formed are less transient. Five amino acid residues and in particular a conserved water molecule contribute to pyrophosphate stabilization. The most important interactions with the enzyme are established with the amino acid residues Arg291β, Lys164α and Lys294β. The amino acid residues Tyr300β and His248β also contribute to the process, however, through significantly more short-lived and weaker hydrogen bonds.

The MD simulations performed together with the available experimental information have also allowed us to propose Tyr361β as the active-site residue that receives the proton from the zinc-bound thiol following peptide coordination in the process that yields the more stable zinc-bound thiolate. More computational and experimental studies are required to fully understand the catalytic mechanism of FTase at the atomic level.

4. Methodology section

The AMBER 8.0[88] molecular dynamics package was used in all the molecular dynamics simulations performed. The systems were prepared for each of the four intermediate states of the FTase catalytic mechanism (Fig. 1) from the crystallographic structures with the best resolution for each state, namely 1FT1 (Enzyme resting state),[56] 1FPP (binary complex FTase-FPP),[69] 1JCR (ternary complex FTase-FPP-Peptide),[70] and 1KZP (product complex).[72] The peptide substrate CVIM from the structure 1D8D[73] was later modelled into the 1JCR active site, at the position of the non-substrate peptide inhibitor CVFM.

Conventional protonation states for all amino acids at pH 7 were considered. All the hydrogen atoms were added and counter-ions (Na+) were employed to neutralize the highly negative charges of the systems (ranging from −20 to −24). The Leap program was used in this regard. The systems were then placed in rectangular boxes containing a minimum distance of 15 Å of TIP3P water molecules between the enzyme and the box side. The size of these four systems was of ca. 140,000 atoms.

Three different sets of parameters[55] specifically designed to allow a reliable treatment of the three different Zn coordination spheres formed during catalysis and based on DFT (B3LYP) and molecular mechanical calculations,[61,63–65] crystallographic data,[56,70,72] extended X-ray absorption fine structure (EXAFS) results,[58] and on several other more recent mechanistic studies[76,83,89,90] were applied to the four-key states of the FTase catalytic pathway. These parameters are described in detail elsewhere, together with the parameterization and validation methods, and with the premises adopted,[55] and have been already used with success in the study of FTase.[65,91,92]

All systems were subjected to a 4-stages refinement protocol using the SANDER module of AMBER 8.0, in which the constraints on the enzyme were gradually removed. In the first stage (10,000 steps), 50 kcal/mol/Å^2 harmonic forces were used to restrain the positions of all atoms in the systems except the ones from the water molecules. In the second stage (10,000 steps) these constraints were applied only to the heavy atoms, and in the third stage (30,000 steps) were limited to the CA and N atom-type atoms (backbone alfa carbons and nitrogens). This process ended in a full energy minimization (4th stage, maximum 80000 steps) until the rms gradient was smaller than 0.02 kcal/mol.

MD simulations on the four systems were carried out using the SANDER module of AMBER 8.0, and considering periodic boundary conditions to simulate a continuous system. The SHAKE algoritm[93] was applied to fix all bond lengths involving a hydrogen bond, permitting a 2-fs time step. The Particle-Mesh Ewald (PME) method[94] was used to include the long-range interactions, and a non-bond-interaction cutoff radius of 10 Å was considered. Following a 40 ps equilibration procedure, 10 ns MD simulations were carried out at 300 K for each of the 4 systems (a total of 40 ns), using Berendsen temperature coupling[95] and constant pressure (1 atm) with isotropic molecule-based scaling. The MD trajectory was sampled every 0.2 ps. All of the MD results were analyzed with the PTRAJ module of AMBER8.0.

Acknowledgment

We thank the FCT (Fundação para a Ciência e a Tecnologia) for financial support (POCI/QUI/61563/2004).

References and notes

1. Chen, W. J.; Andres, D. A.; Goldstein, J. L.; Russell, D. W.; Brown, M. S. *Cell* **1991**, *66*, 327.
2. Moores, S. L.; Schaber, M. D.; Mosser, S. D.; Rands, E.; O'Hara, M. B.; Garsky, V. M.; Marshall, M. S.; Pompliano, D. L.; Gibbs, J. B. *J. Biol. Chem.* **1991**, *266*, 14603.
3. Chen, W. J.; Andres, D. A.; Goldstein, J. L.; Brown, M. S. *Proc. Natl. Acad. Sci. U.S.A.* **1991**, *88*, 11368.
4. Reiss, Y.; Goldstein, J. L.; Seabra, M. C.; Casey, P. J.; Brown, M. S. *Cell* **1990**, *62*, 81.
5. Reiss, Y.; Seabra, M. C.; Armstrong, S. A.; Slaughter, C. A.; Goldstein, J. L.; Brown, M. S. *J. Biol. Chem.* **1991**, *266*, 10672.
6. Schafer, W. R.; Rine, J. *Annu. Rev. Genet.* **1992**, *26*, 209.
7. Glomset, J. A.; Farnsworth, C. C. *Annu. Rev. Cell Biol.* **1994**, *10*, 181.
8. Zhang, F. L.; Casey, P. J. *Annu. Rev. Biochem.* **1996**, *65*, 241.
9. Hancock, J. F.; Magee, A. I.; Childs, J. E.; Marshall, C. J. *Cell* **1989**, *57*, 1167.
10. Jackson, J. H.; Cochrane, C. G.; Bourne, J. R.; Solski, P. A.; Buss, J. E.; Der, C. J. *Proc. Natl. Acad. Sci. U.S.A.* **1990**, *87*, 3042.
11. Kato, K.; Cox, A. D.; Hisaka, M. M.; Graham, S. M.; Buss, J. E.; Der, C. J. *Proc. Natl. Acad. Sci. U.S.A.* **1992**, *89*, 6403.
12. Dolence, J. M.; Poulter, C. D. *Proc. Natl. Acad. Sci. U.S.A.* **1995**, *92*, 5008.
13. Takai, Y.; Sasaki, T.; Matozaki, T. *Physiol. Rev.* **2001**, *81*, 153.
14. Barbacid, M. *Annu. Rev. Biochem.* **1987**, *56*, 779.
15. Bos, J. L. *Cancer Res.* **1989**, *49*, 4682.
16. Almoguera, C.; Shibata, D.; Forrester, K.; Martin, J.; Arnheim, N.; Perucho, M. *Cell* **1988**, *53*, 549.
17. Rodenhuis, S.; Slebos, R. J.; Boot, A. J.; Evers, S. G.; Mooi, W. J.; Wagenaar, S. S.; Van Bodegom, P. C.; Bos, J. L. *Cancer Res.* **1988**, *48*, 5738.
18. Bos, J. L.; Fearon, E. R.; Hamilton, S. R.; Verlaan-de Vries, M.; Van Boom, J. H.; Van der Eb, A. J.; Vogelstein, B. *Nature* **1987**, *327*, 293.
19. Vogelstein, B.; Fearon, E. R.; Hamilton, A. D.; Kern, S. E.; Preisinger, A. C.; Leppert, M.; Nakamura, Y.; White, R.; Smits, A. M.; Bos, J. L. *N. Eng. J. Med.* **1988**, *319*, 525.

20. Huang, C. Y.; Rokosz, L. *Expert Opin. Ther. Patents* **2004**, *14*, 175.
21. Ayral-Kaloustian, S.; Salaski, E. J. *Curr. Med. Chem.* **2002**, *9*, 1003.
22. Ohkanda, J.; Knowles, D. B.; Blaskovich, M. A.; Sebti, S. M.; Hamilton, A. D. *Curr. Top. Med. Chem.* **2002**, *2*, 303.
23. Brunner, T. B.; Hahn, S. M.; Gupta, A. K.; Muschel, R. J.; McKenna, W. G.; Bernhard, E. J. *Cancer Res.* **2003**, *63*, 5656.
24. Caponigro, F.; Casale, M.; Bryce, J. *Expert Opin. Invest. Drugs* **2003**, *12*, 943.
25. Doll, R. J.; Kirschmeier, P.; Bishop, W. R. *Curr. Opin. Drug Discovery Dev.* **2004**, *7*, 478.
26. Adjei, A. A. *Cancer Chemother. Biol. Response Modif.* **2005**, *22*, 123.
27. Kurzrock, R. *Clin. Adv. Hematol. Oncol.* **2005**, *3*, 161.
28. Appels, N. M. G. M.; Beijnen, J. H.; Schellens, J. H. M. *Oncologist* **2005**, *10*, 565.
29. Sousa, S. F.; Fernandes, P. A.; Ramos, M. J. *Curr. Med. Chem.* **2008**, *15*, 1478.
30. Rao, S.; Cunningham, D.; de Gramont, A.; Scheithauer, W.; Smakal, M.; Humblet, Y.; Kourteva, G.; Iveson, T.; Andre, T.; Dostalova, J.; Illes, A.; Belly, R.; Perez-Ruixo, J. J.; Park, Y. C.; Palmer, P. A. *J. Clin. Oncol.* **2004**, *22*, 3950.
31. Van Cutsem, E.; van de Velde, H.; Karasek, P.; Oettle, H.; Vervenne, W. L.; Szawlowski, A.; Schoffski, P.; Post, S.; Verslype, C.; Neumann, H.; Safran, H.; Humblet, Y.; Perez Ruixo, J.; Ma, Y.; Von Hoff, D. *J. Clin. Oncol.* **2004**, *22*, 1430.
32. Sparano, J. A.; Moulder, S.; Kazi, A.; Vahdat, L.; Li, T.; Pellegrino, C.; Munster, P.; Malafa, M.; Lee, D.; Hoschander, S.; Hopkins, U.; Hershman, D.; Wright, J. J.; Sebti, S. M. *J. Clin. Oncol.* **2006**, *24*, 3018.
33. Johnston, S. R. D.; Hickish, T.; Ellis, P.; Houston, S.; Kelland, L.; Dowsett, M.; Salter, J.; Michiels, B.; Perez-Ruixo, J. J.; Palmer, P.; Howes, A. *J. Clin. Oncol.* **2003**, *21*, 2492.
34. Head, J.; Johnston, S. R. D. *Breast Cancer Res.* **2004**, *6*, 262.
35. Rowinsky, E. K. *J. Clin. Oncol.* **2006**, *24*, 2981.
36. Chakrabarti, D.; Da Silva, T.; Barger, J.; Paquette, S.; Patel, H.; Patterson, S.; Allen, C. M. *J. Biol. Chem.* **2002**, *277*, 42066.
37. Wiesner, J.; Kettler, K.; Sakowski, J.; Ortmann, R.; Katzin, A.; Kimura, E.; Silber, K.; Klebe, G.; Jomaa, H.; Schlitzer, M. *Angew. Chem., Int. Ed.* **2004**, *43*, 251.
38. Kettler, K.; Wiesner, J.; Silber, K.; Haebel, P.; Ortmann, R.; Sattler, I.; Dahse, H. M.; Jomaa, H.; Klebe, G.; Schlitzer, M. *Eur. J. Med. Chem.* **2005**, *40*, 93.
39. Eastman, R. T.; White, J.; Hucke, O.; Bauer, K.; Yokoyama, K.; Nallan, L.; Chakrabarti, D.; Verlinde, C. L. M. J.; Gelb, M. H.; Rathod, P. K.; Van Voorhis, W. C. *J. Biol. Chem.* **2005**, *280*, 13554.
40. Glenn, M. P.; Chang, S. Y.; Hucke, O.; Verlinde, C. L.; Rivas, K.; Horney, C.; Yokoyama, K.; Buckner, F. S.; Pendyala, P. R.; Chakrabarti, D.; Gelb, M.; Van Voorhis, W. C.; Sebti, S. M.; Hamilton, A. D. *Angew. Chem., Int. Ed.* **2005**, *44*, 4903.
41. Nallan, L.; Bauer, K. D.; Bendale, P.; Rivas, K.; Yokoyama, K.; Horney, C. P.; Pendyala, P. R.; Floyd, D.; Lombardo, L. J.; Williams, D. K.; Hamilton, A.; Sebti, S.; Windsor, W. T.; Weber, P. C.; Buckner, F. S.; Chakrabarti, D.; Gelb, M. H.; Van Voorhis, W. C. *J. Med. Chem.* **2005**, *48*, 3704.
42. Yokoyama, K.; Trobridge, P.; Buckner, F. S.; Van Voorhis, W. C.; Stuart, K. D.; Gelb, M. H. *J. Biol. Chem.* **1998**, *273*, 26497.
43. Buckner, F. S.; Yokoyama, K.; Nguyen, L.; Grewal, A.; Erdjument-Bromage, H.; Tempst, P.; Strickland, C. L.; Xiao, L.; Van Voorhis, W. C.; Gelb, M. H. *J. Biol. Chem.* **2000**, *275*, 21870.
44. Ohkanda, J.; Buckner, F. S.; Lockman, J. W.; Yokoyama, K.; Carrico, D.; Eastman, R.; Luca-Fradley, K.; Davies, W.; Croft, S. L.; Van Voorhis, W. C.; Gelb, M. H.; Sebti, S. M.; Hamilton, A. D. *J. Med. Chem.* **2004**, *47*, 432.
45. Buckner, F. S.; Eastman, R. T.; Nepomuceno-Silva, J. L.; Speelmon, E. C.; Myler, P. J.; Van Voorhis, W. C.; Yokoyama, K. *Mol. Biochem. Parasitol.* **2002**, *122*, 181.
46. Esteva, M. I.; Kettler, K.; Maidana, C.; Fichera, L.; Ruiz, A. M.; Bontempi, E. J.; Andersson, B.; Dahse, H. M.; Haebel, P.; Ortmann, R.; Klebe, G.; Schlitzer, M. *J. Med. Chem.* **2005**, *48*, 7186.
47. Hucke, O.; Gelb, M. H.; Verlinde, C. L.; Buckner, F. S. *J. Med. Chem.* **2005**, *48*, 5415.
48. Ibrahim, M.; Azzouz, N.; Gerold, P.; Schwarz, R. T. *Int. J. Parasitol.* **2001**, *31*, 1489.
49. Nguyen, U. T. T.; Cramer, J.; Gomis, J.; Reents, R.; Gutierrez-Rodriguez, M.; Goody, R. S.; Alexandrov, K.; Waldmann, H. *Chembiochem* **2007**, *8*, 408.
50. Sousa, S. F.; Fernandes, P. A.; Ramos, M. J. *J. Biol. Inorg. Chem.* **2005**, *10*, 3.
51. Lenevich, S.; Xu, J. H.; Hosokawa, A.; Cramer, C. J.; Distefano, M. D. *J. Am. Chem. Soc.* **2007**, *129*, 5796.
52. Degraw, A. J.; Hast, M. A.; Xu, J. H.; Mullen, D.; Beese, L. S.; Barany, G.; Distefano, M. D. *Chem. Biol. Drug Des.* **2008**, *72*, 171.
53. Cornell, W. D.; Cieplak, P.; Bayly, C. I.; Gould, I. R.; Merz, K. M.; Fergunson, D. M.; Spellmeyer, D. C.; Fox, T.; Caldwell, J. W.; Kollman, P. A. *J. Am. Chem. Soc.* **1995**, *117*, 5179.
54. Weiner, S. J.; Kollman, P. A.; Case, D. A.; Singh, U. C.; Ghio, C.; Alagona, G.; Profeta, S.; Weiner, P. *J. Am. Chem. Soc.* **1984**, *106*, 765.
55. Sousa, S. F.; Fernandes, P. A.; Ramos, M. J. *Theor. Chem. Acc.* **2007**, *117*, 171.
56. Park, H. W.; Boduluri, S. R.; Moomaw, J. F.; Casey, P. J.; Beese, L. S. *Science* **1997**, *275*, 1800.
57. Tamames, B.; Sousa, S. F.; Tamames, J.; Fernandes, P. A.; Ramos, M. J. *Proteins* **2007**, *69*, 466.
58. Tobin, D. A.; Pickett, J. S.; Hartman, H. L.; Fierke, C. A.; Penner-Hahn, J. E. *J. Am. Chem. Soc.* **2003**, *125*, 9962.
59. McCall, K. A.; Huang, C. C.; Fierke, C. A. *J. Nutr.* **2000**, *130*, 1437.
60. Vallee, B. L.; Auld, D. S. *Proc. Natl. Acad. Sci. U.S.A.* **1990**, *87*, 220.
61. Sousa, S. F.; Fernandes, P. A.; Ramos, M. J. *Biophys. J.* **2005**, *88*, 483.
62. Rardin, R. L.; Bino, A.; Poganiuch, P.; Tolman, W. B.; Liu, S.; Lippard, S. J. *Angew. Chem., Int. Ed. Engl.* **1990**, *102*, 812.
63. Sousa, S. F.; Fernandes, P. A.; Ramos, M. J. *J. Mol. Struct. (Theochem)* **2005**, *729*, 125.
64. Sousa, S. F.; Fernandes, P. A.; Ramos, M. J. *J. Comput. Chem.* **2007**, *28*, 1160.
65. Sousa, S. F.; Fernandes, P. A.; Ramos, M. J. *Proteins* **2007**, *66*, 205.
66. Sousa, S. F.; Fernandes, P. A.; Ramos, M. J. *J. Am. Chem. Soc.* **2007**, *129*, 1378.
67. Cui, G.; Merz, K. M. *Biochemistry* **2007**, *46*, 12375.
68. Cui, G. L.; Wang, B.; Merz, K. M. *Biochemistry* **2005**, *44*, 16513.
69. Dunten, P.; Kammlott, U.; Crowther, R.; Weber, D.; Palermo, R.; Birktoft, J. *Biochemistry* **1998**, *37*, 7907.
70. Long, S. B.; Hancock, P. J.; Kral, A. M.; Hellinga, H. W.; Beese, L. S. *Proc. Natl. Acad. Sci. U.S.A.* **2001**, *98*, 12948.
71. Mirza, U. A.; Chen, G. D.; Liu, Y. H.; Doll, R. J.; Girijavallabhan, V. M.; Ganguly, A. K.; Pramanik, B. N. *J. Mass Spectrom.* **2008**, *43*, 1393.
72. Long, S. B.; Casey, P. J.; Beese, L. S. *Nature* **2002**, *419*, 645.
73. Long, S. B.; Casey, P. J.; Beese, L. S. *Struct. Fold Des.* **2000**, *8*, 209.
74. Hightower, K. E.; Huang, C. C.; Casey, P. J.; Fierke, C. A. *Biochemistry* **1998**, *37*, 15555.
75. Huang, C. C.; Casey, P. J.; Fierke, C. A. *J. Biol. Chem.* **1997**, *272*, 20.
76. Pickett, J. S.; Bowers, K. E.; Hartman, H. L.; Fu, H. W.; Embry, A. C.; Casey, P. J.; Fierke, C. A. *Biochemistry* **2003**, *42*, 9741.
77. Rozema, D. B.; Poulter, C. D. *Biochemistry* **1999**, *38*, 13138.
78. Wu, Z.; Demma, M.; Strickland, C. L.; Radisky, E. S.; Poulter, C. D.; Le, H. V.; Windsor, W. T. *Biochemistry* **1999**, *38*, 11239.
79. Strickland, C. L.; Windsor, W. T.; Syto, R.; Wang, L.; Bond, R.; Wu, Z.; Schwartz, J.; Le, H. V.; Beese, L. S.; Weber, P. C. *Biochemistry* **1998**, *37*, 16601.
80. Dolence, J. M.; Rozema, D. B.; Poulter, C. D. *Biochemistry* **1997**, *36*, 9246.
81. Kral, A. M.; Diehl, R. E.; deSolms, S. J.; Williams, T. M.; Kohl, N. E.; Omer, C. A. *J. Biol. Chem.* **1997**, *272*, 27319.
82. Fu, H. W.; Beese, L. S.; Casey, P. J. *Biochemistry* **1998**, *37*, 4465.
83. Pickett, J. S.; Bowers, K. E.; Fierke, C. A. *J. Biol. Chem.* **2003**, *278*, 51243.
84. Del Villar, K.; Mitsuzawa, H.; Yang, W.; Sattler, I.; Tamanoi, F. *J. Biol. Chem.* **1997**, *272*, 680.
85. Spence, R. A.; Hightower, K. E.; Terry, K. L.; Beese, L. S.; Fierke, C. A.; Casey, P. J. *Biochemistry* **2000**, *39*, 13651.
86. Del Villar, K.; Urano, J.; Guo, L.; Tamanoi, F. *J. Biol. Chem.* **1999**, *274*, 27010.
87. Njoroge, F. G.; Vibulbhan, B.; Pinto, P.; Strickland, C.; Bishop, W. R.; Nomeir, A.; Girijavallabhan, V. *Bioorg. Med. Chem. Lett.* **2006**, *16*, 984.
88. Case, D. A.; Darden, T. A.; Cheatham III, T. E.; Simmerling, C. L.; Wang, J.; Duke, R. E.; Luo, R.; Merz, K. M.; Wang, B.; Pearlman, D. A.; Crowley, M.; Brozell, S.; Tsui, V.; Gohlke, H.; Mongan, J.; Hornak, V.; Cui, G.; Beroza, P.; Schafmeister, C.; Caldwell, J. W.; Ross, W. S.; Kollman, P. A. AMBER 8, University of California: San Francisco, 2004.
89. Bowers, K. E.; Fierke, C. A. *Biochemistry* **2004**, *43*, 5256.
90. Hartman, H. L.; Bowers, K. E.; Fierke, C. A. *J. Biol. Chem.* **2004**, *279*, 30546.
91. Sousa, S. F.; Fernandes, P. A.; Ramos, M. J. *J. Phys. Chem. B* **2008**, *112*, 8681.
92. Sousa, S. F.; Fernandes, P. A.; Ramos, M. J. *Int. J. Quantum Chem.* **2008**, *108*, 1939.
93. Ryckaert, J. P.; Ciccotti, G.; Berendsen, H. C. *J. Comput. Phys.* **1977**, *23*, 327.
94. Essman, V.; Perera, L.; Berkowitz, M. L.; Darden, T.; Lee, H.; Pedersen, L. G. *J. Chem. Phys.* **1995**, *103*, 8577.
95. Berendsen, H. C.; Postma, J. P. M.; van Gunsteren, W. F.; DiNola, A.; Haak, J. R. *J. Comput. Phys.* **1984**, *81*, 3684.